ELSEVIER

International Journal of Heat and Fluid Flow 20 (1999) 405–413

International Journal of HEAT AND FLUID FLOW

www.elsevier.com/locate/ijhff

Apex angle effects on the swirling flow between cones induced by means of a tangential inlet

M.N. Noui-Mehidi [a], A. Salem [a], P. Legentilhomme [b,*], J. Legrand [b]

[a] *LMF-IP USTHB, B.P. 32 El-Alia, B.P. 32 Algiers, Algeria*

[b] *Laboratoire de Génie des Procédés, IUT, Département Génie Chimique, B.P. 420, 44606 Saint-Nazaire Cedex, France*

Received 17 May 1998; accepted 11 February 1999

Abstract

A numerical resolution of the laminar swirling flow between two fixed cones having the same apex angle is presented in the case where the fluid is tangentially introduced at the system base. The resolution of the momentum and continuity equations is done by using an implicit finite different scheme. Two conical configurations are considered. In the first one, named CG1, the apex of the cones generatrix is located at the top with respect to the fluid entrance, in the second one, named CG2, the apex is down. The calculations, which concern the three components of the velocity flow-field and the pressure, allowed us to compare the swirl properties in the two studied situations with respect to a similar system made of two coaxial cylinders. The swirl intensity, calculated from the velocity field revealed that in the CG1 case the swirling motion is stronger and the swirl decay is delayed in comparison with the CG2 and the cylindrical cases. © 1999 Elsevier Science Inc. All rights reserved.

Keywords: Swirling decaying flow; Apex angle; Laminar flow regime; Numerical simulation; Concentric truncated cones; Finite difference

Notation

$A = R_1/e$	gap ratio
CG1	cones with apex at the exit with respect to the inlet
CG2	cones with apex at the entrance with respect to the inlet
D_i	diameter of the tangential inlet (m)
$e = R_2 - R_1$	gap width (m)
K	dimensionless vortex constant
P'	pressure (Pa)
P	dimensionless pressure
P_0	mean pressure at the entrance (Pa)
Q_v	volumic flow rate ($m^3\ s^{-1}$)
r', θ, z'	polar cylindrical coordinates (m, rad, m)
R_1	maximum radius of the inner cone (m)
R_2	maximum radius of the outer cone (m)
$Re = eU_0/v$	Reynolds number
Sn	swirl intensity, Eq. (20)
u', v', w'	velocity components in the directions z', r', θ ($m\ s^{-1}$)
u, v, w	dimensionless velocity components
U_0	mean velocity in the tangential inlet ($m\ s^{-1}$)
$\bar{w}$	mean tangential velocity in the entrance section of the annular gap ($m\ s^{-1}$)

Greek

γ	cross flow section ratio, Eq. (34)
$\varepsilon = \xi/\Delta\xi$	axial mesh size ratio
η'	radial dimensional transformed coordinate (m)
η	radial dimensionless transformed coordinate
v	kinematic viscosity ($m\ s^{-1}$)
ξ'	axial dimensional transformed coordinate (m)
ξ	axial dimensionless transformed coordinate
ρ	density ($kg\ m^{-3}$)
τ	swirl enhancement ratio, Eq. (33)
ϕ	apex angle (degrees)

1. Introduction

Swirling flows in tubular and annular configurations have been the subject of numerous experimental and theoretical works (Talbot, 1954; Korjack, 1985; Reader-Harris, 1994). The interest in this kind of flow motion is motivated by the fact that several industrial applications use swirling flows to give favorable characteristics to the considered process. The design of different apparatus such as heat exchangers, chemical reactors, separators, takes into account the swirl properties, and best performing configurations are found to be cylindrical gaps. The swirl between two cylinders could be produced by rotating one of the cylinders while an axial flow is superimposed (Coney and El-Shaarawi, 1974), or by using one or several tangential inlets managed at the system base, the cylinders being kept stationary. In this second configuration, it

* Corresponding author. E-mail: legenti@iutsn.univ-nantes.fr

0142-727X/99/$ – see front matter © 1999 Elsevier Science Inc. All rights reserved.
PII: S0142-727X(99)00026-0

has been found that transfer coefficients could be five times greater than those obtained in purely axial developed flows on the inner cylinder of the device (Legentilhomme and Legrand, 1991) and ten times at the outer core (Lefèbvre et al., 1998), the main drawback being that the swirling motion decays rapidly along the flow path.

The swirl characteristics can be modified in special configurations which present some geometrical advantages (Colgan and Terril, 1989). The use of conical pieces of material in different processes, especially where the fluid is rotating, allows one to increase the centrifugal effects in the flow. A conical gap configuration has been used in several applications, the centrifugal effects being more interesting than those of a cylindrical one. Troshkin (1973) has analytically calculated the three dimensional laminar flow-field between rotating cones with the same apex angle using boundary layer simplifications and has discussed the increase of the centrifugal properties when the apex angle is varied. Bark et al. (1984) have numerically studied the motion of two immiscible liquids of different densities in a constant gap between cones both rotating at the same angular velocity. They have found that the flow is divided in two layers, in the first one, the motion of the fluid is similar to that of a non-rotating freely falling film, whereas in the second layer, a kind of rotating-modified Couette–Poiseuille flow with no net volume flux is obtained. Experimentally, Wimmer (1995) has investigated the stability of the flow between conical cylinders having the same apex angle, the inner one being rotated and the outer one at rest. He has discussed the hydrodynamical conditions of the appearance of Taylor vortices and spirals between the cones with regard to the variation of the gap ratio.

Only few works are dedicated to swirling flows in conical configurations induced without any rotating piece of material. Benisek et al. (1990) have experimentally studied the swirling motion in a conical diffuser, the fluid being introduced axially. The present work is concerned with a numerical study of a swirling flow between two truncated stationary cones having the same apex angle, the fluid inlet being tangential at the system base. Two configurations are considered. In the first one, denoted CG1, the apex of the conical generatrix is at the top of the flow system, and in the second one, called CG2, the apex is down. The comparison of the swirl properties in the two conical configurations is done with regard to a classical cylindrical annular gap in the same conditions.

2. Basic equations

The steady basic flow of an incompressible fluid of constant physical properties is considered in the two flow systems presented in Fig. 1. The swirl induced by a single tangential inlet is not axisymmetric, such as that between rotating cylinders with axial flow, but several authors assumed this kind of flow to be almost axisymmetric in the laminar basic motion (Talbot, 1954; Coney and El-Shaarawi, 1974; Terhmina and Mojtabi, 1980; Legentilhomme and Legrand, 1993). On the other hand, in the entrance region, the evolution of the velocity field is much larger in the radial direction than in the axial one, the radial velocity component being smaller than the two other components.

Taking into account these assumptions and applying the usual boundary layer simplifications by checking the order of magnitude of each term in the governing equations, the following system of partial differential equations has been considered by several authors (Coney and El-Shaarawi, 1974;

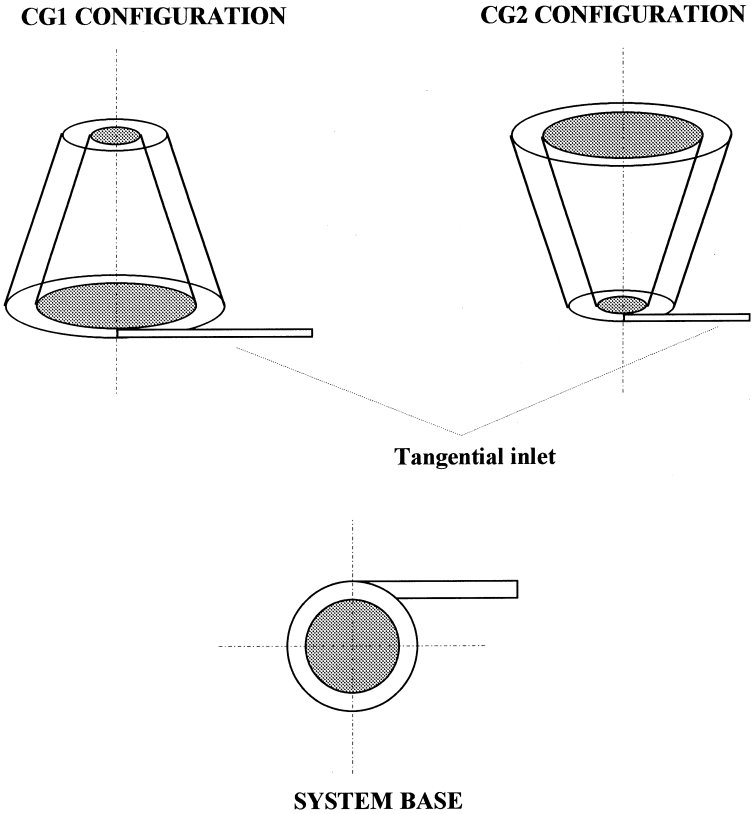

Fig. 1. Flow systems representations.

Terhmina and Mojtabi, 1980; Legentilhomme and Legrand, 1993):

$$\frac{w'^2}{r'} = \frac{1}{\rho}\frac{\partial P'}{\partial r'}, \tag{1}$$

$$v'\frac{\partial w'}{\partial r'} + u'\frac{\partial w'}{\partial z'} + \frac{v'w'}{r'} = \upsilon\left[\frac{\partial^2 w'}{\partial r'^2} + \frac{1}{r'}\frac{\partial w'}{\partial r'} - \frac{w'}{r'^2}\right], \tag{2}$$

$$v'\frac{\partial u'}{\partial r'} + u'\frac{\partial u'}{\partial z'} = -\frac{1}{\rho}\frac{\partial P'}{\partial z'} + \upsilon\left[\frac{\partial^2 u'}{\partial r'^2} + \frac{1}{r'}\frac{\partial u'}{\partial r'}\right], \tag{3}$$

$$\frac{\partial v'}{\partial r'} + \frac{v'}{r'} + \frac{\partial u'}{\partial z'} = 0. \tag{4}$$

The boundary conditions are represented by the no-slip at the conical walls and the inlet properties. In most of the numerical studies concerned with swirling flows in cylindrical geometries, uniform profiles of the axial velocity component, u', and constant pressure, P', at the entrance are assumed (Legentilhomme and Legrand, 1993). Although there is no derivative of v' with respect to the axial direction z', an initial condition on v' is needed in the calculations. Different authors assumed that $v' = 0$ at the entrance (Legentilhomme and Legrand, 1993; Coney and El-Shaarawi, 1974; Terhmina and Mojtabi, 1980). The initial profile of w' at the entrance depends on the type of vortex motion imposed at the inlet. For swirling decaying annular flows, the vortex is often chosen of forced type, either when a tangential inlet Legentilhomme and Legrand, 1993) or a rotating inlet section (Talbot, 1954) is used to induce the swirling motion. Thus the inlet tangential velocity profile can be expressed by: $w' = Cr'$, where C is a constant which characterizes the intensity of the initial tangential motion.

3. Domain of calculation

The axial variation of the conical radii induced a difficulty in specifying constant boundary conditions on the walls in polar cylindrical coordinates. A coordinate transformation allows one to transform the conical gap in each of the two cases CG1 and CG2 to a cylindrical gap which could be easily meshed. This analytical and unique transformation is mathematically conformal (Arfken, 1970). The two domains related to CG1 and CG2 are transformed to rectangular ones as depicted in Fig. 2.

The transformation f_1 for CG1 is given by

$$f_1: \begin{vmatrix} \eta' = r' + z'\tan\left(\frac{\phi}{2}\right) \\ \xi' = z' \end{vmatrix} \tag{5}$$

where ϕ is the apex angle.

The transformation f_2 for CG2 is

$$f_2: \begin{vmatrix} \eta' = r' - z'\tan\left(\frac{\phi}{2}\right) \\ \xi' = z' \end{vmatrix} \tag{6}$$

The boundary conditions, in the two transformed systems of coordinates, are given by:

$$\begin{aligned} &\eta' = \eta'_1 = R_1: \quad u' = v' = w' = 0, \\ &\eta' = \eta'_2 = R_2: \quad u' = v' = w' = 0. \end{aligned} \tag{7}$$

The derivatives take then the forms:

$$\text{CG1:} \begin{vmatrix} \frac{\partial}{\partial r'} = \frac{\partial}{\partial \eta'} \\ \frac{\partial}{\partial z'} = \frac{\partial}{\partial \xi'} + \tan\left(\frac{\phi}{2}\right)\frac{\partial}{\partial \eta'} \end{vmatrix} \tag{8}$$

$$\text{CG2:} \begin{vmatrix} \frac{\partial}{\partial r'} = \frac{\partial}{\partial \eta'} \\ \frac{\partial}{\partial z'} = \frac{\partial}{\partial \xi'} - \tan\left(\frac{\phi}{2}\right)\frac{\partial}{\partial \eta'} \end{vmatrix} \tag{9}$$

Replacing these derivatives in the system of Eqs. (1)–(4), we obtain two new systems of equations for CG1 and CG2 configurations, respectively.

4. Dimensionless formulation

For the resolution of the obtained partial differential equations systems, the following dimensionless quantities have been introduced:

$$\begin{aligned} &\eta = \frac{\eta' - \eta'_1}{e}, \quad \xi = \frac{\xi'}{e}, \quad \mathrm{Re} = \frac{eU_0}{\upsilon}, \quad A = \frac{R_1}{e}, \\ &u = \frac{u'}{U_0}, \quad v = \frac{v'}{U_0}, \quad w = \frac{w'}{U_0}, \quad P = \frac{P' - P'_0}{\rho U_0^2}. \end{aligned} \tag{10}$$

Applying the coordinates transformation and these dimensionless quantities to Eqs. (1)–(4), we obtain the following systems to be solved for the CG1 configuration:

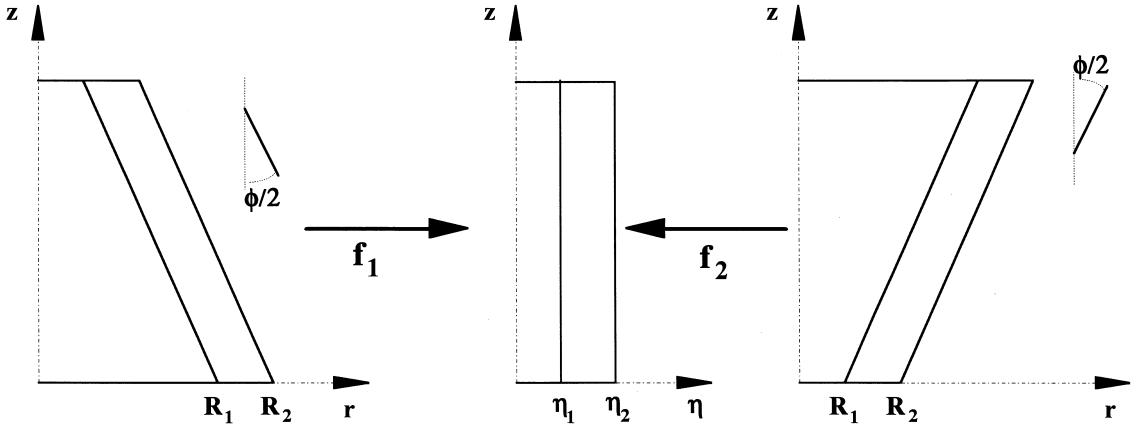

Fig. 2. Coordinates transformation and domain of calculations.

$$\frac{w^2}{\eta + A - \xi\tan\left(\frac{\phi}{2}\right)} = \frac{\partial P}{\partial \eta}, \tag{11}$$

$$\left(v + u\tan\left(\frac{\phi}{2}\right)\right)\frac{\partial w}{\partial \eta} + u\frac{\partial w}{\partial \xi} + \frac{uw}{\eta + A - \xi\tan\left(\frac{\phi}{2}\right)} = \frac{1}{\mathrm{Re}}\left[\frac{\partial^2 w}{\partial \eta^2} + \frac{1}{\eta + A - \xi\tan\left(\frac{\phi}{2}\right)}\frac{\partial w}{\partial \eta} - \frac{w}{\left(\eta + A - \xi\tan\left(\frac{\phi}{2}\right)\right)^2}\right], \tag{12}$$

$$\left(v + u\tan\left(\frac{\phi}{2}\right)\right)\frac{\partial u}{\partial \eta} + u\frac{\partial u}{\partial \xi} + \tan\left(\frac{\phi}{2}\right)\frac{w^2}{\eta + A - \xi\tan\left(\frac{\phi}{2}\right)} = -\frac{\partial P}{\partial \xi} + \frac{1}{\mathrm{Re}}\left[\frac{\partial^2 u}{\partial \eta^2} + \frac{1}{\eta + A - \xi\tan\left(\frac{\phi}{2}\right)}\frac{\partial u}{\partial \eta}\right], \tag{13}$$

$$\frac{\partial v}{\partial \eta} + \frac{v}{\eta + A - \xi\tan\left(\frac{\phi}{2}\right)} + \tan\left(\frac{\phi}{2}\right)\frac{\partial u}{\partial \eta} + \frac{\partial u}{\partial \xi} = 0. \tag{14}$$

For the CG2 case, the system of equations to solve can be easily obtained by replacing ϕ by $-\phi$ in Eqs. (11)–(14).

One can notice that putting $\phi = 0$ in these two systems leads to the same set of equations corresponding to a classical cylindrical annular configuration. This property allows the validation of the numerical results in comparison with those obtained by Legentilhomme and Legrand (1993), and a comparison of the swirl characteristics in the conical cases with those of the cylindrical one. At the fluid entrance, the momentum in the annular section is supposed to be only expressed by an angular component. Considering the flow rate conservation at the entrance, we assume that the ratio between the mean velocity in the tangential inlet of diameter D_i and the annular velocity at $\xi = 0$ in the annular gap is given by the ratio $4D_i[R_2 - R_1]/\pi D_i^2$, where $D_i[R_2 - R_1]$ represents the admission section of the fluid in the annular gap, supposed to be a rectangle of height D_i and base $e = R_2 - R_1$ (Legentilhomme and Legrand, 1993). The dimensionless inlet forced vortex is given by:

$$w = \frac{w'}{U_0} = \frac{CR_2}{U_0}\eta\big|_{\xi=0}. \tag{15}$$

Integrating Eq. (15) between η_1 and η_2 and using the expression of the mean dimensionless tangential velocity in the entrance section of the annular gap, $\bar{w}$, we obtain:

$$\overline{w} = \frac{Q_v}{eD_iU_0} = \frac{\pi(R_2^2 - R_1^2)U_0}{eD_iU_0} = \frac{CR_2}{U_0}\frac{1}{\eta_2|_{\xi=0} - \eta_1|_{\xi=0}}\int_{\eta_1|_{\xi=0}}^{\eta_2|_{\xi=0}} \eta\,\mathrm{d}\eta, \tag{16}$$

where Q_v is the volumic flow rate.

Finally, C is given the following equation:

$$C = \frac{2\pi U_0}{D_i} \tag{17}$$

and the entrance profile of the angular velocity component in the annular gap by:

$$w = \frac{2\pi R_2}{D_i}\eta\big|_{\xi=0} = K\eta\big|_{\xi=0}. \tag{18}$$

According to Eq. (18), the initial swirl intensity can be adjusted by changing the diameter, D_i, of the tangential inlet duct. An increase in Reynolds number, by means of the volumic flow rate, will also induce a modification of the mean dimensional inlet angular velocity, w'.

The boundary and inlet conditions resume to:

$$\begin{aligned} &\xi = 0, \quad \text{whatever } \eta\text{: } u = 1,\ v = 0,\ w = K\eta,\ P = 0,\\ &\xi > 0\text{:} \begin{cases} \eta = 0\text{: } u = v = w = 0,\\ \eta = 1\text{: } u = v = w = 0. \end{cases} \end{aligned} \tag{19}$$

The swirling flow characteristics are described by the swirl intensity which is defined in the transformed domain by Clayton and Morsi (1984):

$$\mathrm{Sn} = \frac{\int_0^1 uw\eta^2\,\mathrm{d}\eta}{\int_0^1 u^2\eta\,\mathrm{d}\eta} \tag{20}$$

and corresponds to the ratio between the angular and axial momentum fluxes at a given axial position.

5. Numerical solution

The finite difference method used hereafter has been successfully checked by several authors interested in swirling and rotating flows in cylindrical configurations. The implicit scheme used here is derived from the one of Coney and El-Shaarawi (1974). The finite differences used in the calculations have been treated in detail in a previous work related to a conical gap (Noui-Mehidi and Salem, 1997). The systems of partial differential equations (11)–(14) are transformed to linear algebraic systems represented by:

for the CG1 case:

$$B_i^1 w_{i-1,j+1} + B_i^2 w_{i,j+1} + B_i^3 w_{i+1,j+1} = B_i^4, \tag{21}$$

$$w_{i,j+1}^2 = \frac{A + i\Delta\eta - j\Delta\xi\tan\left(\frac{\phi}{2}\right)}{\Delta\eta}\left(P_{i,j+1} - P_{i-1,j+1}\right), \tag{22}$$

$$P_{i,j+1} + C_i^1 u_{i-1,j+1} + C_i^2 u_{i,j+1} + C_i^3 u_{i+1,j+1} = C_i^4, \tag{23}$$

$$D_i^1 v_{i+1,j+1} + D_i^2 v_{i,j+1} = D_i^3, \tag{24}$$

for the case CG2, we obtain:

$$B_i^5 w_{i-1,j+1} + B_i^6 w_{i,j+1} + B_i^7 w_{i+1,j+1} = B_i^8, \tag{25}$$

$$w_{i,j+1}^2 = \frac{A + i\Delta\eta - j\Delta\xi\tan\left(\frac{\phi}{2}\right)}{\Delta\eta}\left(P_{i,j+1} - P_{i-1,j+1}\right), \tag{26}$$

$$P_{i,j+1} + C_i^5 u_{i-1,j+1} + C_i^6 u_{i,j+1} + C_i^7 u_{i+1,j+1} = C_i^8, \tag{27}$$

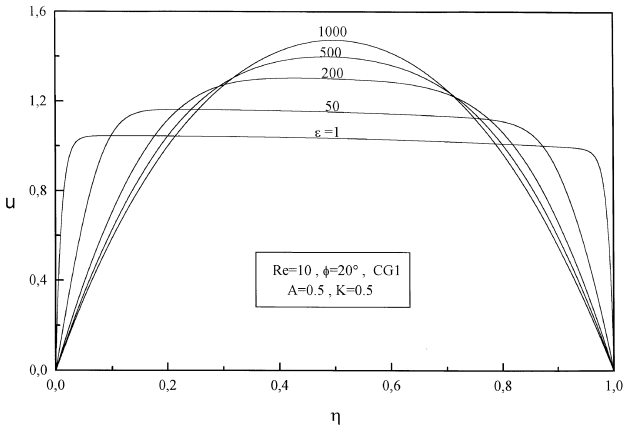

Fig. 3. Axial velocity component evolution – CG1 case.

$$D_i^4 v_{+1,j+1} + D_i^5 v_{i,j+1} = D_i^6. \quad (28)$$

The coefficients B, C and D have different expressions in each case (CG1 and CG2) and are related to variables different from those calculated in the corresponding equation.

An additional equation is needed in the calculations and is introduced from the integral representation of the continuity equation as:

for the CG1 case:

$$\int_0^1 \left(\eta + A - \xi \tan\left(\frac{\phi}{2}\right)\right) u \, d\eta = \frac{1}{8} \quad (29)$$

and for the CG2 case:

$$\int_0^1 \left(\eta + A + \xi \tan\left(\frac{\phi}{2}\right)\right) u \, d\eta = \frac{1}{8}. \quad (30)$$

These last two equations are reduced by the trapezoidal rule of numerical integration:

$$\sum_{i=1}^{N} u_{i,j+1} \left(i\Delta\eta + A - j\Delta\xi \tan\left(\frac{\phi}{2}\right)\right) = \frac{1}{8\Delta\eta}, \quad (31)$$

$$\sum_{i=1}^{N} u_{i,j+1} \left(i\Delta\eta + A + j\Delta\xi \tan\left(\frac{\phi}{2}\right)\right) = \frac{1}{8\Delta\eta}. \quad (32)$$

All the obtained equations are consistent with the boundary layer equations and stable for all mesh sizes only when the axial velocity remains positive, the recirculating flows cannot then be treated. The finite difference equations are linearized by assuming that in the product of two unknowns, one keeps approximately its value at the previous step. Variables with subscript $j+1$ are unknowns and those of subscript j are assumed to be known. The solution of the equation of w (Eq. (21) or (25)) is done by Thomas algorithm, the calculation of u and P (Eqs. (22) and (23) or Eqs. (26) and (27)) is processed using a specific matrix algorithm (Amaouche, 1986) and v is implicitly calculated by solving Eq. (24) or Eq. (28).

6. Results and discussion

The aim of this paper is to compare the effects of symmetry on the swirling flow in the two configurations CG1 and CG2 with regard to the cylindrical one ($\phi = 0$). Thus, numerical simulations were performed for different Reynolds numbers in the range 1 to 30, for gap width and apex angle kept constant

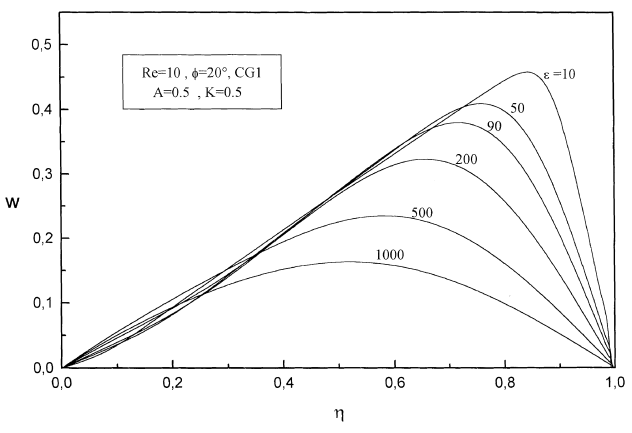

Fig. 4. Tangential velocity component evolution – CG1 case.

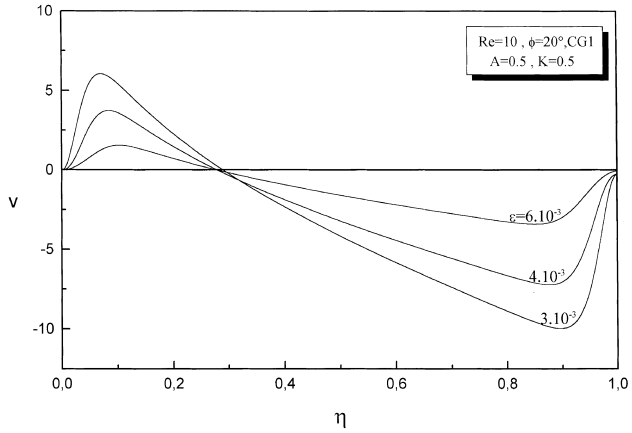

Fig. 5. Radial velocity component evolution – CG1 case.

($A = 0.5$; $\phi = 20°$). The inlet vortex intensity was chosen to be moderate ($K = 0.5$). The mesh sizes employed for these calculations were $\Delta\eta = 10^{-3}$ and $\Delta\xi = 10^{-3}$. In these conditions ($\Delta\xi$ and $\Delta\eta$ less or equal to 10^{-3}), the numerical results have been checked to ensure that they are independent of mesh sizes.

The hydrodynamics of the swirling flow in the case of the CG1 configuration has been the object of a previous work (Noui-Mehidi and Salem, 1997). In Figs. 3–5 we can respectively observe the development of the axial, tangential and radial velocity components. These profiles are given as a function of $\varepsilon = \xi/\Delta\xi$, which represents the number of axial steps from the tangential inlet. The maximum of the axial velocity increases in the downstream direction from the entrance and the axial velocity profile becomes established at $\varepsilon = 1000$. In contrast, the tangential velocity decreases continuously from the entrance region, corresponding to the decay of the swirling motion along the flow path. The radial velocity component evolution points out the development of the two boundary layers on the conical walls from the entrance region, and decreases until it completely vanishes as the flow becomes axially established.

In Fig. 6, the evolution of the axial velocity component is given for the configurations CG1, CG2 and the cylindrical one. At the axial position $\varepsilon = 1000$, we can see that u is greater in the CG2 configuration than in the two other, due to the faster axial flow establishment in the CG2

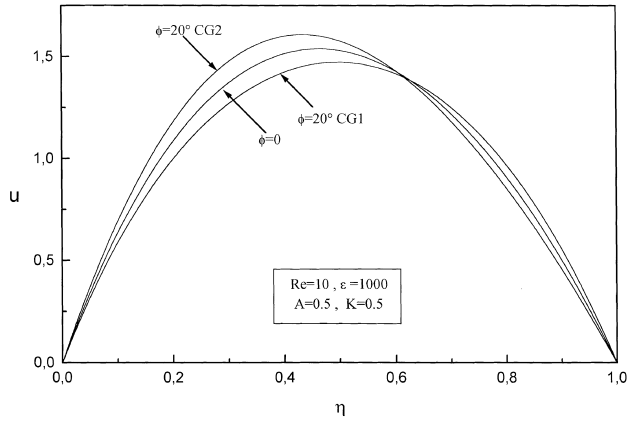

Fig. 6. Comparison of the axial velocity component evolutions between conical configurations and cylindrical one.

configuration. In other hand, the maximum of u is located closer to the outer wall for the case CG1 than for the other two cases.

As expected, the tangential velocity component is much larger in the CG1 case than in the cylindrical or the CG2 configurations. But the evolution is not the same near the entrance region and far from the tangential inlet. For an axial position of $\varepsilon = 500$, as displayed in Fig. 7, we can notice that w is greater in the CG2 than in the two other configurations in the half fluid column close to the inner wall, while in the other half, near the outer wall, the opposite situation occurs and w is greater in the CG1 than in the two other situations. This fact points out that in the neighborhood of the tangential inlet, the swirl characteristics are more sensitive near the outer wall. Far from the entrance region, at $\varepsilon = 1000$, the situation is different. In the entire gap width, w is greater in the CG1 case than in the other configurations especially near the outer wall. Closer to the inner wall, the characteristics of w are rather identical for the three configurations. These differences in the behaviour of u and w from one case to the other could also be observed in the axial variations of the maxima of each velocity component. Figs. 8 and 9 respectively display the variations of the maxima of u and w for a Reynolds number value equal to 10. As we can notice in Fig. 8, while the value of u_{max} becomes constant for a cylindrical situation far from the entrance region, u_{max} slightly increases in CG1 and decreases in CG2. In both cases, u_{max} tends towards a constant value in the transformed systems of coordinates (Fig. 2), corresponding to the maximum axial velocity obtained in cylindrical configuration, only depending on the radii ratio of both cylinders for a given value of the Reynolds number, in absence of tangential motion. Obviously, the maximum axial velocity in conical systems of coordinates does not reach a constant value due to the evolution (increase or decrease) of the radii ratio along the axial direction. In opposite, w_{max} decreases in the same manner in all the situations as illustrated in Fig. 9. The variations of the radial locations of u_{max} and w_{max} in the downstream direction are displayed in Fig. 10. As we can notice, the radial positions of u_{max} and w_{max} for CG1 and CG2 configurations are different. For CG1, these maxima are located closer to the outer wall in comparison with the cylindrical case, while in CG2 they are located closer to the inner wall. For the three configurations, it can be emphasized that the location of the maximum of axial and tangential velocities tends towards the same radial position when the axial distance from the inlet increases, due to the decrease in swirl intensity which induces a flow-field dominated by the axial velocity component.

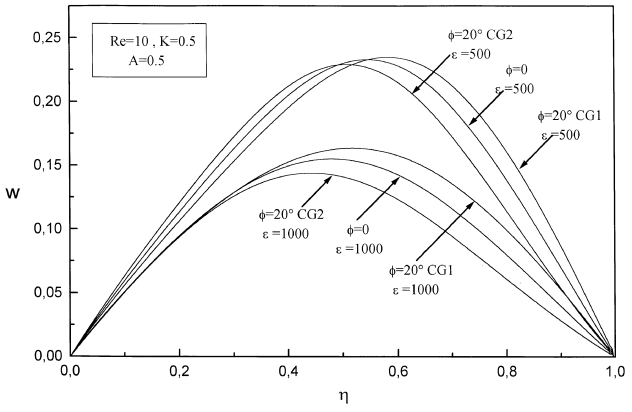

Fig. 7. Comparison of the tangential velocity component evolutions between conical configurations and cylindrical one.

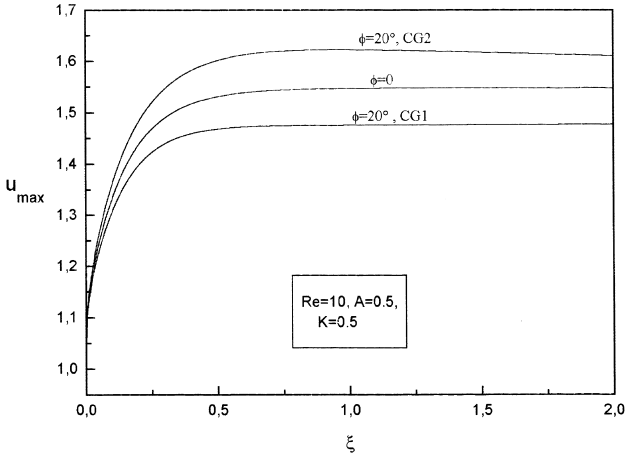

Fig. 8. Evolution of the maximum of the axial velocity component in conical and cylindrical configurations.

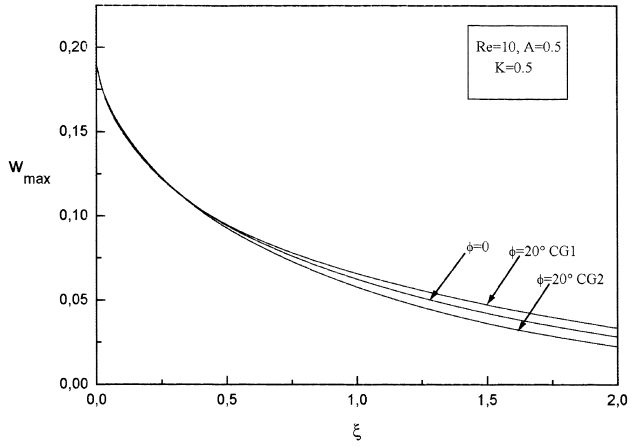

Fig. 9. Evolution of the maximum of the tangential velocity component in conical and cylindrical configurations.

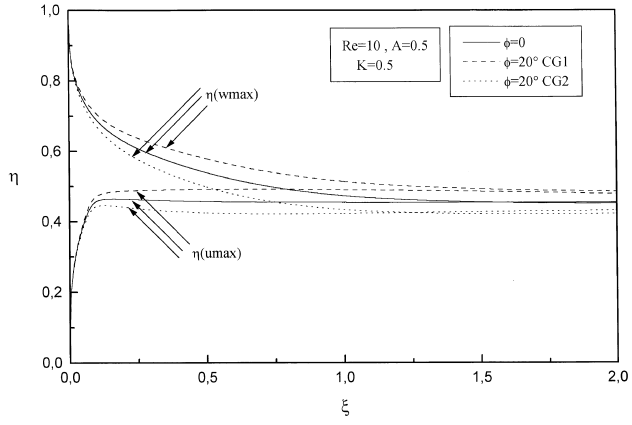

Fig. 10. Axial evolution of the radial locations of the maxima of u and w for conical and cylindrical configurations.

In Fig. 11, the swirl intensity, Sn (Eq. (20)), is represented for the three cases as a function of the reduced axial location ξ. We can notice that from the entrance region, the swirl intensity is much larger in the CG1 case than in the two other systems. This evolution confirms that the swirl characteristics are better in the CG1 situation. The loss of symmetry between the conical situations and the cylindrical one when the Reynolds number increases is clearly displayed for $\mathrm{Re} = 30$, the swirl decay is more pronounced in the CG2 case. In other hand, the evolution of Sn with the axial location from the inlet is of the same kind for the three configurations for a given Reynolds number value.

The swirl properties in CG1 and CG2 configurations, in comparison with those of a pure cylindrical configuration, could be better observed in Fig. 12. This figure gives the axial evolution of the ratio $|\tau/\gamma|$, where τ is the rate of swirl which represents the relative deviation between the swirl intensity in CG1 or CG2 and the one in a cylindrical system, and is expressed by:

$$\tau = \frac{\mathrm{Sn}_{\mathrm{CG1\ or\ CG2}} - \mathrm{Sn}_{\phi=0}}{\mathrm{Sn}_{\phi=0}} \tag{33}$$

and γ represents the flow cross section deviation of CG1 and CG2 configurations with respect to the cylindrical annular geometry ($\phi = 0$):

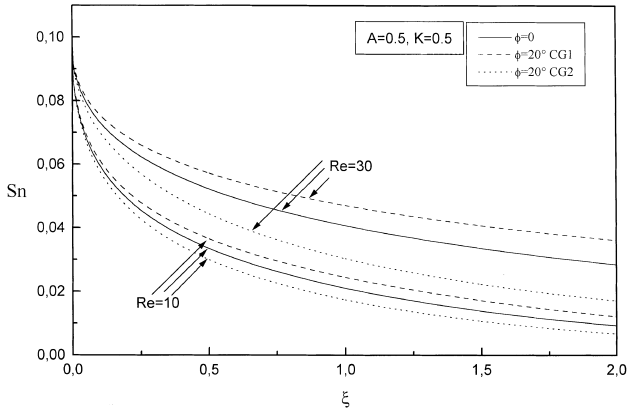

Fig. 11. Swirl intensity evolution.

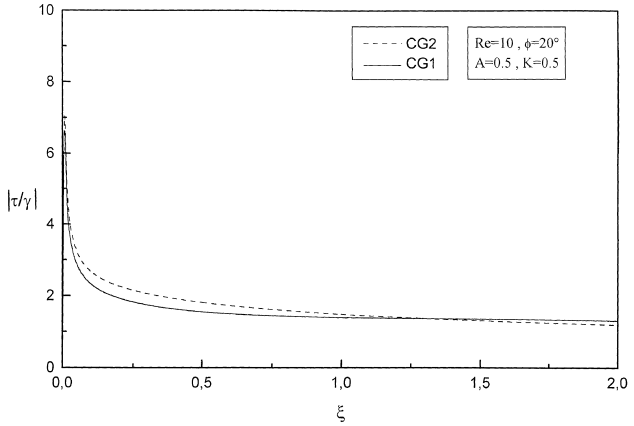

Fig. 12. Evolution of the relationship between the swirl ratio and the cross section deviation in CG1 and CG2 configurations.

$$\gamma = \frac{\left|\pi\left(R_2^2(z) - R_1^2(z)\right)_{\mathrm{CG1\ or\ CG2}} - \pi\left(R_2^2 - R_1^2\right)_{\phi=0}\right|}{\pi\left(R_2^2 - R_1^2\right)_{\phi=0}}. \tag{34}$$

All the obtained flow properties allow one to suppose that the swirl characteristics are not only linked to the geometrical properties. The swirl motion seems to be affected by the hydrodynamics in addition to the change of the flow cross sections in the conical systems. This fact could be observed in Fig. 12. Far from the entrance region, the ratio $|\tau/\gamma|$ is greater than unity. This result reveals that the swirl deviation between conical and cylindrical situations is not only linked to the geometrical changes. Swirl motion induced by a tangential inlet has specific characteristics in conical configurations with respect to the cylindrical geometry.

Laminar flows in annuli or parallel plates are of practical significance because of their potential applications in the processing of industrially important highly viscous or non-Newtonian fluids, such as polymer melts and liquid foods. These fluids are commonly processed under low Reynolds number conditions because of their apperent viscosities and also the small hydraulic diameters used in compact heat exchangers (Etemad et al., 1994). Rotating flows in annular passages may be very interesting in processes involving flows of highly viscous liquids due to the possibility of obtaining large rates of heat or mass transfer with respect to pure axial flow thanks to the combination of axial and tangential velocity components. Swirl flows generated by tangential inlets can be a very simple solution to increase the performance of heat and mass exchangers.

In most experimental and theoretical works dedicated to decaying swirling flows, the swirl number, Sn, is found to decrease exponentially from the entrance section [Bottaro et al. (1991) for a laminar swirling decaying pipe flow induced by a single tangential inlet; Morsi and Clayton (1986) in a swirling annular decaying flow induced by means of guide vanes; Yapici et al. (1994) for swirling decaying annular flow induced by kinetic mixers or Legentilhomme et al. (1993) in swirling annular flow generated by a tangential inlet]. Using the data of Fig. 11, the ratio between the swirling intensity in the conical CG1 configuration, $\mathrm{Sn}_{\mathrm{CG1}}$, to that obtained in a cylindrical annulus, $\mathrm{Sn}_{\phi=0}$, can be correlated as follows:

- $\mathrm{Re} = 10$:

$$\frac{\mathrm{Sn}_{\mathrm{CG1}}}{\mathrm{Sn}_{\phi=0}} = 1.03\exp(0.1075\xi), \tag{35}$$

- $\mathrm{Re} = 30$:

$$\frac{\mathrm{Sn}_{\mathrm{CG1}}}{\mathrm{Sn}_{\phi=0}} = 1.02\exp(0.1362\xi). \tag{36}$$

In a previous work dealing with experimental mass transfer in swirling decaying annular flow induced by means of a tangential inlet, Legentilhomme et al. (1993) have found that, in the laminar flow regime ($100 \leqslant \mathrm{Re} \leqslant 1000$), the ratio between the Sherwood number, $\mathrm{Sh}_{\phi=0}$, in swirling flow, to that determined by Turitto (1975) in fully developed laminar axial flow, $\mathrm{Sh}_{\mathrm{ax}}$, is given by:

$$\frac{\mathrm{Sh}_{\phi=0}}{\mathrm{Sh}_{\mathrm{ax}}} = 1 + 0.33S_0^{0.12}\left[\frac{2e}{L_1 + \ell_{\mathrm{e}}}\right]^{-0.03}\left[1 + \frac{L_1}{\ell_{\mathrm{e}}}\right]^{-0.91}. \tag{37}$$

In Eq. (37), S_0 represents the initial swirl intensity defined by Legentilhomme and Legrand (1991):

$$S_0 = \frac{4(1+N)}{1-N}\left[\frac{e}{D_{\mathrm{i}}}\right]\mathrm{Re} \tag{38}$$

with $N = R_1/R_2$. In Eq. (37), ℓ_{e} is the length of the transfer surface, L_1 being the distance between the tangential inlet and

the leading edge of this transfer section. Sh_{ax}, the overall Sherwood number on the inner cylinder, between two axial locations, L_1 and L_2, in fully developed axial flow is given (Turitto, 1975) by:

$$Sh_{ax} = [2ef(N)Re\ Sc]^{1/3}\left[\frac{L_2^{2/3} - L_1^{2/3}}{L_2 - L_1}\right] \tag{39}$$

with

$$f(N) = \frac{2[-2N^2 + (1-N^2)/\ln(1/N)][(1-N)/N]}{1 + N^2 - (1-N^2)/\ln(1/N)}. \tag{40}$$

For an annular gap with of 7×10^{-3} m ($R_2 = 25 \times 10^{-3}$ m, $R_1 = 18 \times 10^{-3}$ m), a Schmidt number, $Sc = 1255$, corresponding to an experimental configuration previously studied by Legentilhomme et al. (1993), and for a mass transfer section located just downstream the tangential inlet ($L_1 = 0$) and of length, ℓ_e, equal to 0.028 m, corresponding to a dimensionless length, ζ, equal to 2, Eq. (37) predicts a Sherwood number equal to 56 and 89 for Re equal to 10 and 30 respectively. For this evaluation, we assume that Eq. (37) established by Legentilhomme et al. (1993) for Reynolds number values greater than 100 can by extrapolated for smaller Re. The enhancement in mass transfer in swirling annular decaying flow compared with a fully developed laminar axial flow is respectively equal to 65% and 79% for Re equal to 10 and 30.

Integration of Eqs. (35) and (36) from $\xi = 0$ to $\xi = 2$, leads to a mean value of the ratio $Sn_{GC1}/Sn_{\phi=0}$ equal to 1.15 and 1.17 for a Reynolds number value equal to 10 and 30, respectively. In first approximation, we can assume that the part

$$0.33 S_0^{0.12}\left[\frac{2e}{L_1 + \ell_e}\right]^{-0.03}\left[1 + \frac{L_1}{\ell_e}\right]^{-0.91}$$

of Eq. (37) is proportional to the mean swirl intensity over the length of the transfer section, in cylindrical geometry, and that in the conical one, the influence of the swirl intensity on the overall mass transfer will follow the same tendency. Thus, using the average value of $Sn_{GC1}/Sn_{\phi=0}$, Eq. (37) will lead to Sherwood numbers equal to 60 and 92 in the CG1 configuration respectively for $Re = 10$ and $Re = 30$. These values represent an enhancement in overall mass transfer respectively equal to 75% and 87% in comparison with that obtained in fully developed axial flow and 15% and 10%, respectively with respect to cylindrical swirling flows. It seems that the enhancement of mass transfer rate due to the conical shape decreases with an increase in Reynolds number. It means that the conical arrangement would be particularly interesting for the processing of very highly viscous fluids.

7. Conclusion

The numerical results obtained in the different studied configurations for tangential inlet-induced-flow pointed out that the swirling properties are more interesting in the CG1 configuration than in the cylindrical or the CG2 ones. The increase of the swirl intensity in all the situations in the CG1 makes this configuration favourable to processes needing stronger and maintained swirling motions. However, the characteristics of the swirling flow are not only related to the change of the cross flow sections in the conical cases. The conical geometry induces a swirling flow pattern different from that given by the cylindrical one.

The CG1 configuration appears very promising from an industrial point of view, especially for processes involving mass or heat transfer in highly viscous fluids such as that encountered in food industry for instance, operating at very low Reynolds numbers.

References

Amaouche, M., 1986. Contribution à l'étude de la convection mixte externe. Doctorat-Es-Sciences thesis, Poitiers University, France.

Arfken, G., 1970. Mathematical Methods for Physicists. Academic Press, New York.

Bark, F.H., Johanson, A.V., Carlson, C.G., 1984. Axisymmetric stratified two-layer flow in a rotating conical channel. Journal de Mécanique Théorique et Appliquée 3, 861–878.

Benisek, M., Nedjeljkvic, M., Cantrak, S., 1990. An investigation on the incompressible turbulent swirling flow characteristics change along straight conical diffuser. Z. Angew. Math. Mech. T 70 (5), 456–458.

Bottaro, A., Ryhminig, I.L., Wehrili, M.B., Rys, F.S., Rys, P., 1991. Laminar swirling flow and vortex breakdown in a pipe. Comput. Methods Appl. Mech. Eng. 89, 41–57.

Clayton, B.R., Morsi, Y.S.M., 1984. Determination of principal characteristics of turbulent swirling flow along annuli. Part 1 – Measurement of time mean parameters. Int. J. Heat Fluid Flow 5 (4), 195–203.

Colgan, T., Terril, R.M., 1989. An investigation of some axisymmetric flows through circular pipes of slowly changing radius. Int. J. Eng. Sci. 27 (4), 433–440.

Coney, J.E.R., El-Shaarawi, M.A.I., 1974. A contribution to numerical solution of developing laminar flow in the entrance region of concentric annuli with rotating inner walls. J. Fluid Eng., Trans. ASME, 339–340.

Etemad, S.Ch., Mujumdar, A.S., Huang, B., 1994. Viscous dissipation effects in region heat transfer for power law fluid flowing between parallel plates. Int. J. Heat Fluid Flow 15, 122–131.

Korjack, T.A., 1985. Mass transfer of decaying products in swirling laminar pipe flow. Powder Technology 45, 57–62.

Lefèbvre, G., Farias Neto, S.R., Aouabed, H., Legentilhomme, P., Legrand, J., 1998. Transfert de matière et chute de pression lors d'um écoulement tourbillonnaire non-entretenu induit par une entrée tangentielle. Can. J. Chem. Eng. 79, 1039–1050.

Legentilhomme, P., Legrand, J., 1991. The effects of inlet conditions on mass transfer in annular swirling decaying flow. Int. J. Heat Mass Transfer 34, 1281–1291.

Legentilhomme, P., Legrand, J., 1993. Modélisation numérique du transfert de matière dans un écoulement annulaire faiblement tourbillonnaire non-entretenu. Can. J. Chem. Eng. 71, 299–311.

Legentilhomme, P., Aouabed, P., Legrand, J., 1993. Developing mass transfer in swirling decaying flow induced by means of a tangential inlet. Chem. Eng. J. 52, 137–147.

Morsi, Y.S.M., Clayton, B.R., 1986. Determination of principal characteristics of turbulent swirling flow along annuli. Part 3 – An asymptotic solution. Int. J. Heat Fluid Flow 8 (4), 293–302.

Noui-Mehidi, M.N., Salem, A., 1997. Numerical solution of the laminar flow in the entrance region between conical cylinders with tangential inlet. In: Proceedings of The Tenth International Conference on Numerical Methods in Laminar and Turbulent Flows, vol. 10. Pineridge, Swansea, pp. 323–334.

Reader-Harris, M.J., 1994. The decay of swirl in a pipe. Int. J. Heat Fluid Flow 15, 212–217.

Talbot, L., 1954. Laminar swirling pipe flow. J. Appl. Mech. 21, 1–7.

Terhmina, O., Mojtabi, A., 1980. Ecoulements de convection forcée en régimes dynamique et thermique non établis dans un espace annulaire. Int. J. Heat Mass Transfer 31 (3), 583–590.

Troshkin, O.A., 1973. Calculation of the hydrodynamical characteristics of the flow of a viscous liquid between rotating cones. Teor. Osnovny Khim. Tekhnol. 7, 897–903.

Turitto, V.T., 1975. Mass transfer in annuli under conditions of laminar flow. Chem. Eng. Sci. 30, 503–509.

Wimmer, M., 1995. An experimental investigation of Taylor vortex flow between conical cylinders. J. Fluid Mech. 292, 205–227.

Yapici, S., Patrick, M.A., Wragg, A.A., 1994. Hydrodynamics and mass transfer in decaying annular swirl flow. Int. Commun. Heat Mass Transfer 21, 41–51.